ORIGINAL ARTICLE

Open Access

Cooling and Crack Suppression of Bone Material Drilling Based on Microtextured Bit Modeled on Dung Beetle

Yunsong Lian[1*], Xiande Chen[1], Chaoping Xie[1], Yangyang Long[2], Fengtian Lin[3], Wei Zhou[1] and Xuyang Chu[1]

Abstract

In recent years, the number of patients with orthopedic diseases such as cervical spondylosis has increased, resulting in an increase in the demand for orthopedic surgery. However, thermal necrosis and bone cracks caused by surgery severely restrict the development and progression of orthopedic surgery. For the material of cutting tool processing bone in bone surgery of drilling high temperature lead to cell death, easy to produce the problem such as crack cause secondary damage effects to restore, in this paper, a bionic drill was designed based on the micro-structure of the dung beetle's head and back. The microstructure configuration parameters were optimized by numerical analysis, and making use of the optical fiber laser marking machine preparation of bionic bit; through drilling test, the mathematical model of drilling temperature and crack generation based on micro-structure characteristic parameters was established by infrared thermal imaging technology and acoustic emission signal technology, and the cooling mechanism and crack suppression strategy were studied. The experimental results show that when the speed is 60 m/min, the cooling effects of the bionic bit T1 and T2 are 15.31% and 19.78%, respectively, and both kinds of bits show obvious crack suppression effect. The research in this paper provides a new idea for precision and efficient machining of bone materials, and the research results will help to improve the design and manufacturing technology and theoretical research level in the field of bone drilling tools.

Keywords Bionic drill, Bone material cutting, Laser processing, Thermal imaging camera, Acoustic emission

1 Introduction

Owing to the advancement in science and technology, more scholars are focusing on the investigation of cutting bone materials [1]. However, because bone material is a biologically active material that exhibits inferior thermal conductivity, it can easily cause mechanical and thermal damage to the tissues, blood vessels, and nerves around the bone during the cutting process [2, 3]. Furthermore,

improper cutting can cause cracks in the bone material, cause fatal damage to the bone tissue, and severely hinder a patient's post-operative recovery [4]. Therefore, the cooling mechanism of bone materials cutting tools and the strategy to suppress surface cracks on bone materials must be investigated to improve the quality of bone surgery and accelerate post-operative body recovery [5].

Currently, most researchers are investigating the cooling mechanism and crack suppression of bone materials cutting from the aspect of tool structure and optimized cutting parameters. Bertollo et al. [6] used a two-blade bit and a three-point bit separately to perform a cortical bone drilling experiment, and the characteristics of the heat curve were determined by evaluating each bit when comparing the drilling efficiency and thermal performance; it was discovered that the three-point bit

*Correspondence:
Yunsong Lian
lianys@xmu.edu.cn
[1] Department of Mechanical and Electrical Engineering, Xiamen University, Xiamen 361102, China
[2] Institute of Dynamics and Vibration Research, Leibniz Universität Hannover, 30167 Hannover, Germany
[3] Xiamen Golden Egret Special Alloy Co., Ltd, Xiamen 361100, China

Lian *et al. Chinese Journal of Mechanical Engineering*   (2023) 36:37

Page 2 of 13

drilling efficiency was greater than that of the two-blade bit. However, the three-blade-bit cutting efficiency did not result in less heat production; in fact, it promoted the improvement in the screws for bone healing. Heydari et al. [7] applied the response surface experimental design method to derive a mathematical model for predicting the behavior of process temperature with varying input variables. The effects of individual parameters and their interactions on the output were analyzed, and it was discovered that the process temperature increased with rotational speed; however, it indicated an extreme point as the feed rate increased owing to competing factors of the bone-tool contact time. The process temperature increased owing to the high bone-tool contact time at low feed rates and then increased again because of high forces and friction at high feed rates. Li et al. [8] used finite element software to simulate and analyze the drilling process of bone materials under different processing parameters. The results showed that the drilling temperature increased with the feed speed, bit diameter, and rotational speed. Sugita et al. [9] proposed a cutting method using vibration impact, and the results showed that the main cutting force reduced by more than 80% in each cutting direction. In addition, the method allowed a lower cutting temperature and inhibited bone deformation, although small cracks still occurred.

Currently, studies regarding the cooling mechanism of bone drilling primarily focus on drilling parameters and drill structures, whereas studies regarding the suppression of bone cracks are scarce. Therefore, a new bionic drill based on the dung beetle surface microstructure is proposed herein to improve the drilling technology of bone materials. Additionally, it solves the problems of high temperature and surface cracks during bone drilling.

2 Morphological Topology

Dung beetles travel through soil for many years, and their surface microstructure, particularly the densely arranged head convex structure and back pit structure, can significantly reduce their resistance to travel in soil. Therefore, in this study, the microstructure of the convex hull and pit on the head and back of a dung beetle were applied to the surface of a drill bit. This reduces the contact length between the drill bit and bone material, thereby allowing a lower drilling temperature. However, the friction coefficient between the bit and the bone material effectively reduces the friction force, which inhibits crack propagation along the bond line.

The photograph of a dung beetle is shown in Figure 1. Dung beetles generally measure 20−30 mm long and exhibit a black oval shape with a slight luster. The front of the head is fan-shaped, with protruding sides. The body

**Figure 1** Top view of dung beetle magnification
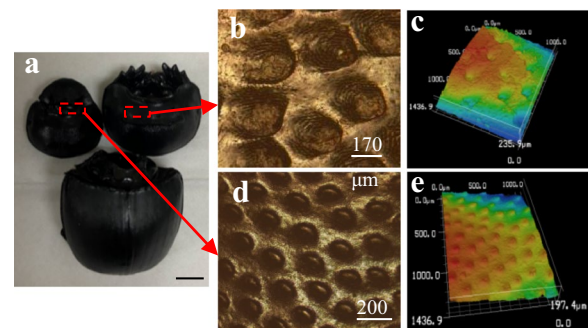
Figure 2 Three-dimensional image of scanned beetle: **a** Dung beetle, **b** local amplification of the back, **c** back three-dimensional scanned, **d** local amplification of the head and **e** head three-dimensional scanned

is of a dark color, and the crown extends to the forehead. Moreover, a sharp corner exists at the center.

In this study, dung beetles were cleaned in distilled water and sterilized in a 95% ethanol solution. Finally, a developer was applied to the body surface of the dung beetles. After the developer was completely dried, scanning was conducted for 3D to extract the convex hull and pit microstructure, as shown in Figure 2.

As shown in Figure 3, the three-dimensional microstructure model was imported into GEOMAGIC software to capture its image and then convert it into space coordinates; subsequently, the point cloud data of the microstructure of the convex hull and pit on the surface of the dung beetle were obtained. The point cloud data was imported into the MATLAB software, and the acquired point cloud data were filtered; the 3D model image obtained is shown in Figure 4. The microstructure parameters of the convex hull and pit are shown in Figures 5 and 6, respectively.

The seven microstructures of the major axis of the ellipse, minor axis of the ellipse, and height of the convex hull in the microstructure of the convex hull, as well as the major axis of the ellipse, minor axis of the ellipse, pit depth, and distance from the lowest point of the pit

Lian *et al. Chinese Journal of Mechanical Engineering*   (2023) 36:37

Page 3 of 13
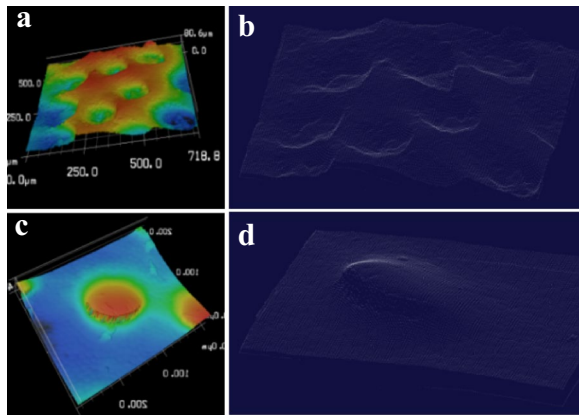
Figure 3 Point cloud data on surface of dung beetles: **a** Convex hulls (front), **b** convex hulls (reverse), **c** pits (front) and **d** pits (reverse)
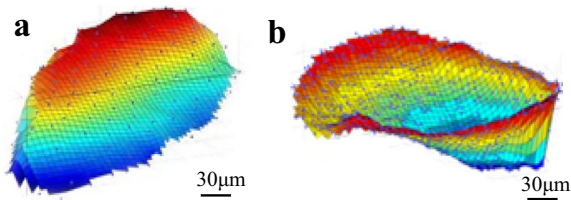
Figure 4 Reconstructed 3D model image on surface of dung beetle: **a** Convex hulls and **b** pits
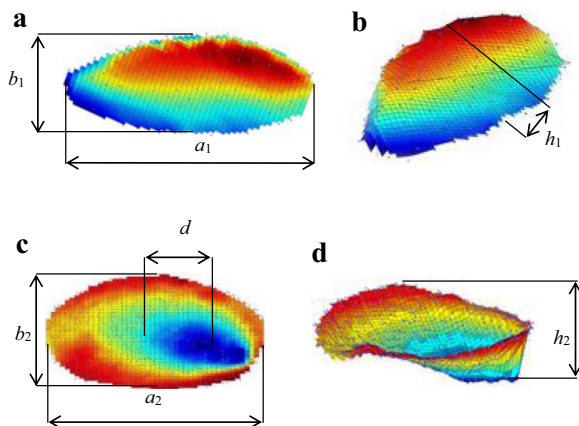
Figure 5 Description of microstructure parameters: **a** Convex hulls vertical view, **b** convex hulls front view, **c** pits vertical view, **d** pits front view

to the center of the ellipse in the pit microstructure were designed. Abaqus finite element software was used to carry out orthogonal test, and the boundary setting, mesh division and temperature cloud map of simulation are shown in Figure 7. Figure 8 shows the trend diagram of the influence of various factors on drilling temperature.

Based on this, normal bit (NT) without microtexture was used as the control, bit T1 with the least cutting force and bit T2 with the least cutting temperature are selected for subsequent tests, and their parameters are shown in Table 1.

3 Experiment

3.1 Drill Bit Preparation

The drill bit material used in the test was an M35 high-speed steel twist drill, and the relevant geometric parameters with their values are listed in Table 2. The bionic drill bits were processed using an RFL-100W series fiber laser marking machine, and the processing parameters and their values are shown in Table 3. Prior to laser processing, the drill bit was manually ground, mechanically polished, and then ultrasonically cleaned twice in alcohol. Subsequently, metallographic sandpaper was used to polish the surface and edges of the material to thoroughly remove impurities and burrs, and then deep cleaning was performed via ultrasonication. The processing device is illustrated in Figure 8. Laser processing technology was used to prepare bionic microstructured drill bits T1 and T2, as shown in Figure 9. The microtexture morphology, pit depth and convex hull height were observed by laser scanning microscope, as shown in Figure 10.

3.2 Drilling Experiments

Figure 11 shows a schematic diagram of the bone material drilling test. CNC machine drill bits were used to perform the bone drilling tests. By installing twist drills to process the bone material, the uniformity of the feed and the consistency of the processing time were ensured. The site layout of the drilling test is illustrated in Figure 12.

4 Result Discussion

4.1 Theoretical Analysis

During drilling, a significant amount of friction was generated among the tool, bone material, and bone chips, resulting in high heat at the contact point [10, 11]. Owing to heat accumulation, the uneven heating of bone materials resulted in inconsistent thermal expansion and thermal stress cracks [12]. As drilling is a semi-closed process, the bone chips can be bonded easily to the tool. In addition to the tool feed, the chip particles on the front tool surface contribute to extrusion on the surface of the bone material. This effect of the bonding line between the bone units will affect the material bonding line and produce defects that gradually expand into cracks [13]. The drilling heat and crack sources associated with the drilling are shown in Figure 13.

The main cause of drilling heat and cracks is the high friction between the drill bit and the bone material; therefore, friction generated during drilling should be

Lian *et al. Chinese Journal of Mechanical Engineering*   (2023) 36:37

Page 4 of 13
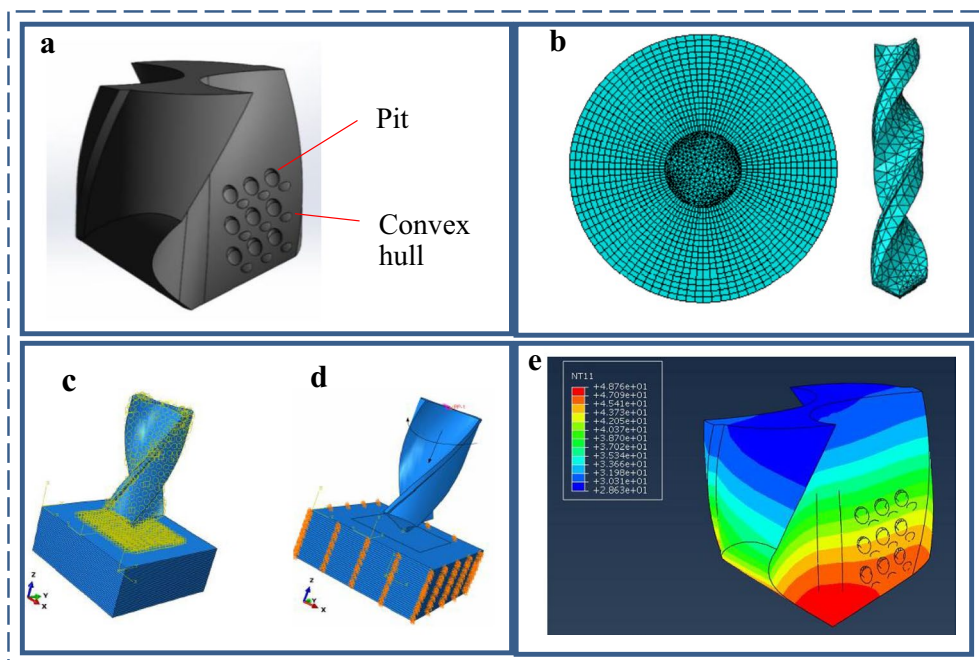
Figure 6 Abaqus drilling simulation: **a** Composite microtextured bit, **b** mesh, **c** contact, **d** boundary conditions and **e** cloud map of temperature field distribution

reduced [14]. This study was based on the microtexture of the head and back of dung beetle. Pits, first can shorten the knife-contact length, thereby reducing friction between the bit and chip; second, they can store the chips after fracture and effectively reduce the amount of chips to the bone material force. Furthermore, the convex hull functions as a good chip breaker with potholes can effectively inhibit the formation of cracks.

4.2 Drilling Force

During drilling, a KISTLER piezoelectric dynamometer was used to measure the cutting force at a sampling frequency of 15 kHz. From a macroscopic point of view, bone material is mainly affected by axial force. However, radial force will also be generated due to the tool vibration easily caused by fracture cutting mode and the incline of the tool head to a certain extent in the process of drilling. The friction between the bit and chip was determined by the positive stress on the knife-chip contact surface. In other words, the drilling force, particularly the axial force, determined the amount of friction [15]. The average values of the axial and radial forces in the steady drilling state were extracted as the test results, and the change trends of both forces as a function of the cutting speed are shown in Figure 14.

At cutting speeds of 20−60 m/min, the axial and radial forces of the three drill bits decreased as the cutting speed increased. In fact, the axial and radial forces of

typical cutting drill bits decrease from 70.53 and 20.32 N to 40.18 and 14.27 N, respectively. The convex and concave microstructures of the two groups of bionic drill bits reduced the contact area and contact length of the helical cutting surface and the bone material. Consequently, the positive pressure and shear force on the contact surface reduced, the axial and radial forces reduced significantly as compared with those of the ordinary knife, and the friction between the knife and chip reduced significantly.

The axial and radial forces of T1 reduced from 63.125 and 19.14 N to 29.34 and 11.34 N, respectively, and the reduction percentage increased from 10.50% and 4.95% to 36.98% and 20.53%, respectively, compared with typical drill bits. The axial and radial forces of T2 reduced from 65.3 and 19.3 N to 25.19 and 10.19 N, respectively, and the reduction percentage increased from 7.42% and 0.99% to 37.3% and 28.59%, respectively, compared with typical drill bits.

4.3 Drilling Temperature

During drilling process, the cutting temperature generated by drilling is mainly caused by the heat on the shear surface and the friction heat between the cutter and the chip, a portable thermal imaging camera was used to monitor the drill bit tip temperature in real time [16, 17]. Additionally, the difference in cutting temperature between the bionic drill bits and the typical drill bits at the tip were compared and analyzed.

Lian *et al. Chinese Journal of Mechanical Engineering*   (2023) 36:37

Page 5 of 13
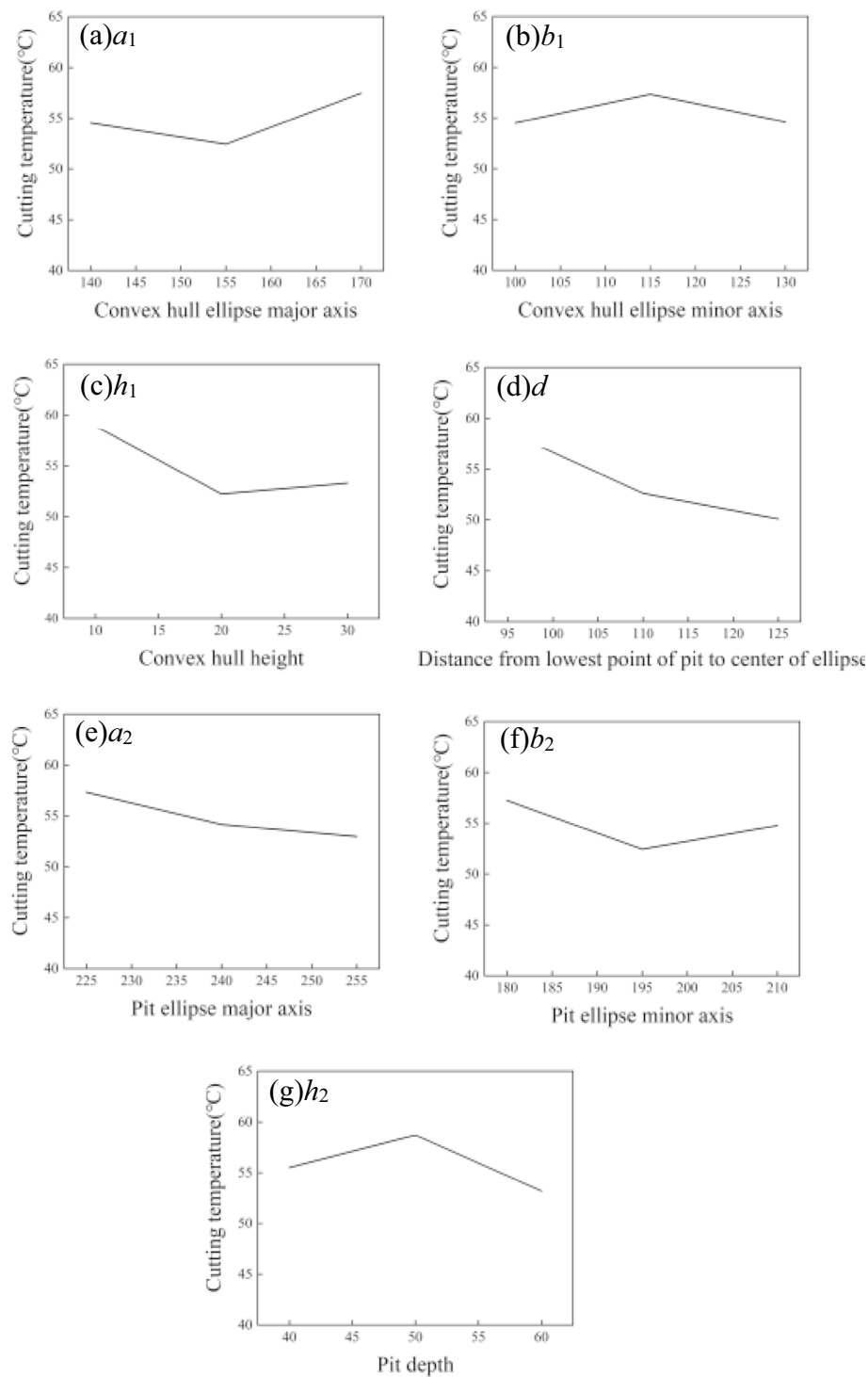
Figure 7 Effect trend chart of seven factors

Under a cutting speed $v_c = 40$ m/min and feed speed $v_f = 30$ mm/min, the infrared thermography of the bionic drill bits (T1 and T2) and typical drill bit (NT) of the dry cutting bone material is shown in Figure 15. At this time, the maximum temperatures of the above mentioned drill bits at the tool-chip contact area were 45.0 °C, 49.7 °C, and 56.0 °C, respectively.
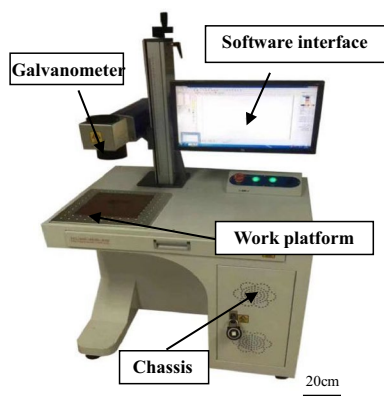
Figure 8 Fiber laser marking machine

Table 1 Orthogonal test plan for cutting simulation

| Parameter (µm)	T1	T2
Convex hull ellipse major axis a_1	140	155
Convex hull ellipse minor axis b_1	100	130
Convex hull height h_1	10	20
Distance from lowest point of pit to center of ellipse d	95	125
Pit ellipse major axis a_2	225	255
Pit ellipse minor axis b_2	180	195
Pit depth h_2	40	60

Table 2 Geometric parameters of drill bits and their values

Parameter	Value
Vertex (°)	135
Helix angle (°)	30
Blade inclination (°)	55
Diameter (mm)	4.2

Table 3 Laser processing parameters

Parameter	Value range
Average output power P (W)	10
Repeat frequency f (kHz)	10
Scan speed v (mm/s)	100
Number of scan n	3

Figure 16 shows a bar graph of the cutting temperature changes of the three drill bits in the range of $v_f = 20-60$ mm/min cutting speed. In the range of $v_c = 20-60$ m/min, the cutting temperature of the three drill bits increased with the cutting speed. Compared with the trend chart of the drilling force, although the drilling
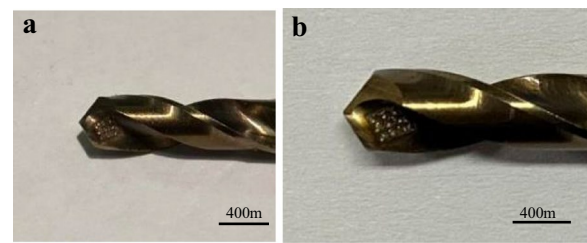
**Figure 9** Bionic microtexture drill bits: **a** T1 and **b** T2

force decreased as the cutting speed increased, the cutting temperature increased. This is primarily because drilling is a semi-closed process, and the thermal conductivity of cortical bone materials is inferior; therefore, the heat generated during processing cannot dissipate easily.

The drilling temperature of the typical drill bit increased from 42.1 to 62.7 °C, whereas the bionic drill bit, owing to the presence of pits, not only reduced the contact length between the cutter and chip, which directly reduced the heat generated by friction, but was also conducive to chip discharge, thereby increasing the heat dissipation efficiency. The temperatures of T1 and T2 increased from 37.5 °C and 36.6 °C to 50.3 °C and 53.1 °C, respectively. Evidently, their heating range was much smaller than that of ordinary drills. The cooling effects of the two bionic bits increased from 5.94% and 7.93% to 15.31% and 19.78%, respectively.

4.4 Drilling Cracks
In the process of drilling, if the bone material cracks, the crack direction will be between the bone unit or the vertical tear layer between the bone unit and the matrix, the crack direction is consistent with the axial force direction; combined with the front end signal voltage mean trend chart and axial force trend chart at different cutting speeds, it can be judged that the crack generation has a significant relationship with axial force. The PXAEX3.0 system was used to receive the acoustic emission signal; in fact, the acoustic emission signal during drilling can be obtained, analyzed, played back, and exported in real time, it is applied to monitor and locate the damage behavior by detecting the sudden release of energy in the loading process [18, 19]. Acoustic emission energy is released rapidly owing to the deformation of the bone materials. The higher the acoustic emission energy, the higher the energy release rate of the material deformation is, and the more likely bone cracks will occur [20, 21]. The acoustic emission energy output results of the three drills at cutting speed $v_c = 20-60$ m/min (feed speed $v_f = 30$ mm/min) are shown in Figure 17.

At any cutting speed, from the beginning of drilling to approximately 0.8 s, the drill bit drilled the bone unit fiber side at the entrance. The bone unit fiber was subjected to
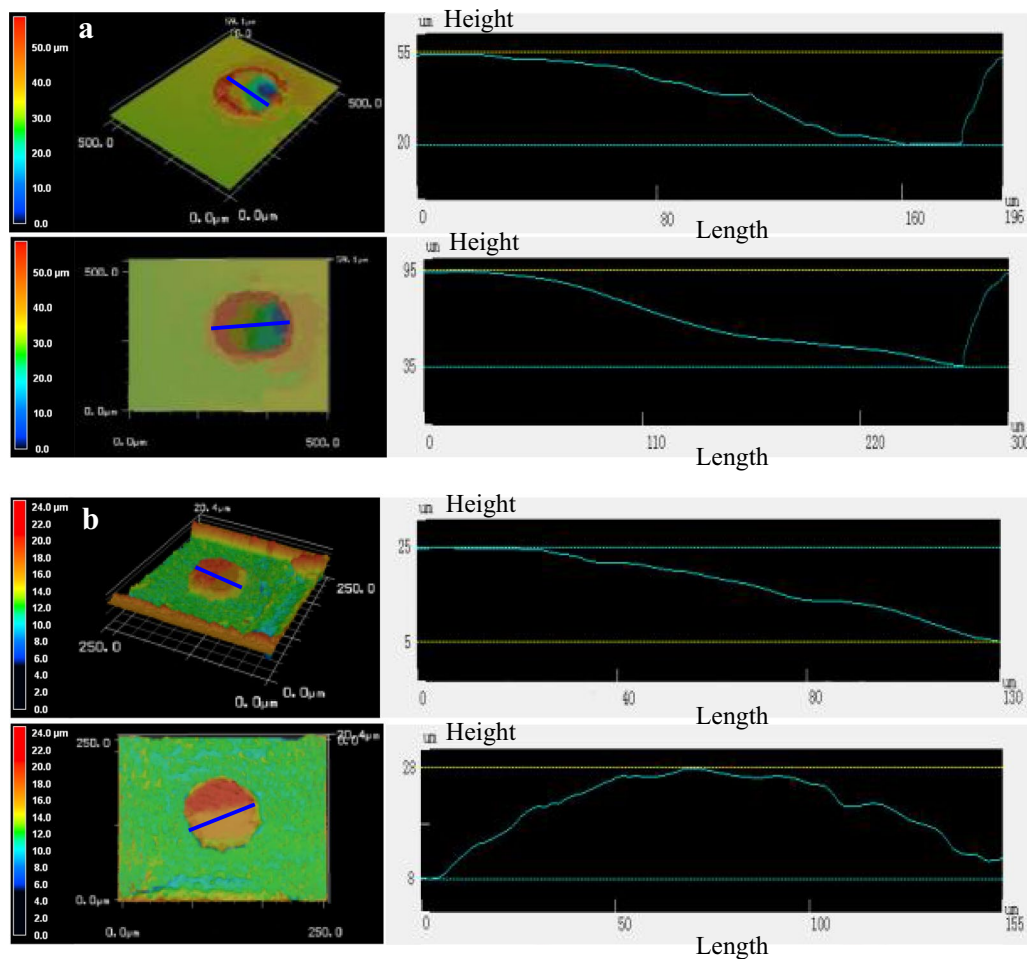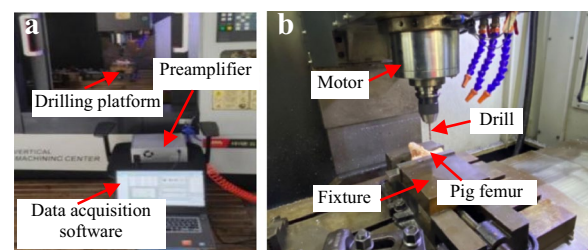
Figure 10 Laser scanning microscope images of microtextured bit: **a** Pits and **b** convex hull
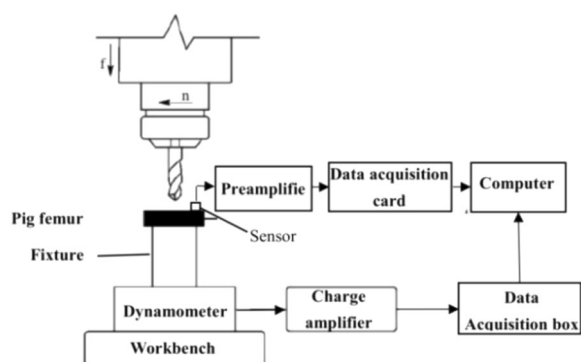
Figure 11 Schematic diagram of drilling test

Figure 12 Site layout drawing of drilling test: **a** Front view and **b** left 45° view
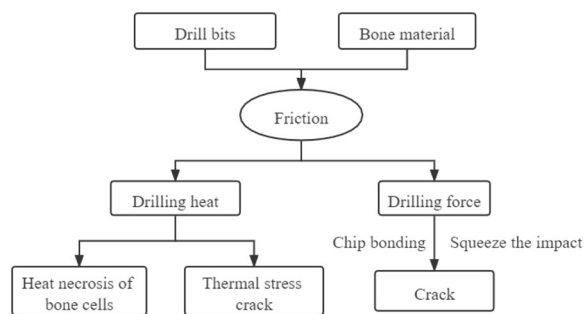
a high axial force, and shear stress along the axial tangential linear velocity direction was generated between the bone unit fiber and the undrilled region below the drill bit. Therefore, the drilling process was extremely unstable, resulting in a significant amount of acoustic emission energy. However, the voltage amplitude decreased after 0.8 s because the drilling stabilized as the bit continued to drill.
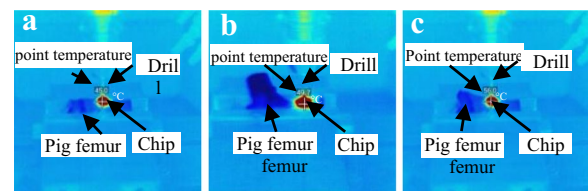
The most volatile region was concentrated at the front end, which was prone to bone cracking. Therefore, data processing was performed on the front end signal, and the average voltage between the start drilling time of 0.25
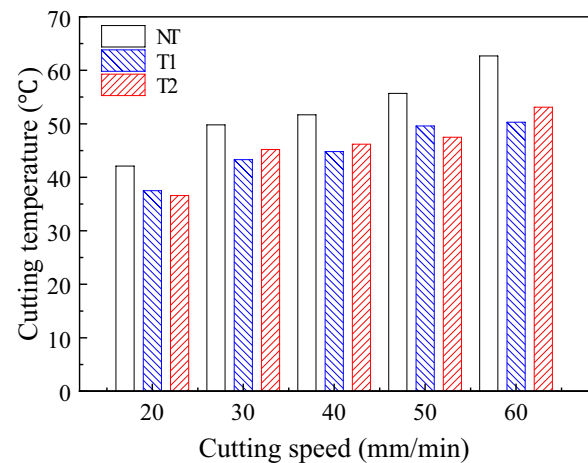
Figure 13 Diagram of drilling heat and crack sources

Figure 15 Infrared thermal images of three drill bits during dry cutting of bone materials (v_c= 40 m/min and feed speed v_f = 30 mm/min): **a** T2, **b** T1 and **c** NT

s and steady drilling time of 0.8 s was used as the test result data and then compared and analyzed, as shown in Figure 18.

In the range of v_c = 20−60 m/min, the voltages of the three bits decreased as the speed increased. The voltage of the regular bit reduced from 286.76 to 150.28 mV. The bionic drill chuck demonstrated good chip breaking ability; the pit exhibited good chip storage ability, which reduced the impact of extrusion; and the measured voltage value was considerably lower than that of an ordinary drill. The voltages of T1 and T2 decreased from 262.18 and 253.46 mV to 60.34 and 75.12 mV, respectively. Compared with typical bits, their voltage signal reduction ratios increased from 8.57% and 11.61% to 59.81% and 50.01%, respectively. In addition, The suppression of cracks mainly depends on the reduction of the contact area between the helical cutting surface and the workpiece and the reduction of the positive pressure and shear force on the contact surface, which leads to the reduction of the friction coefficient, the squeezing and scratching
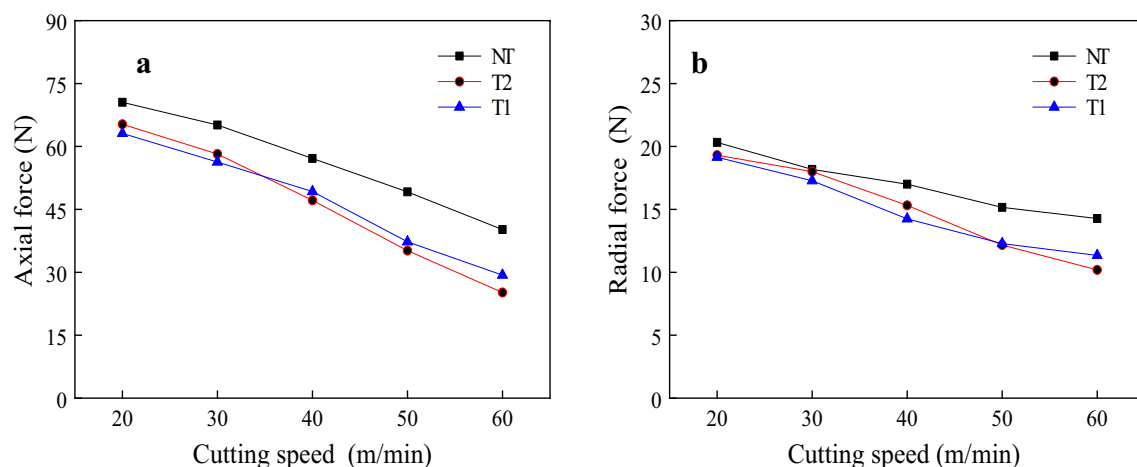

Figure 16 Cutting temperature changes of three drill bits at different cutting speeds

caused by chips, and the reduction of the energy release rate of material deformation. As the processing goes on, the bone chips will gradually accumulate in the pits, making the pit depth decreases, and the

Figure 14 Trends of axial and radial forces as a function of cutting speed: **a** Axial force and **b** radial force
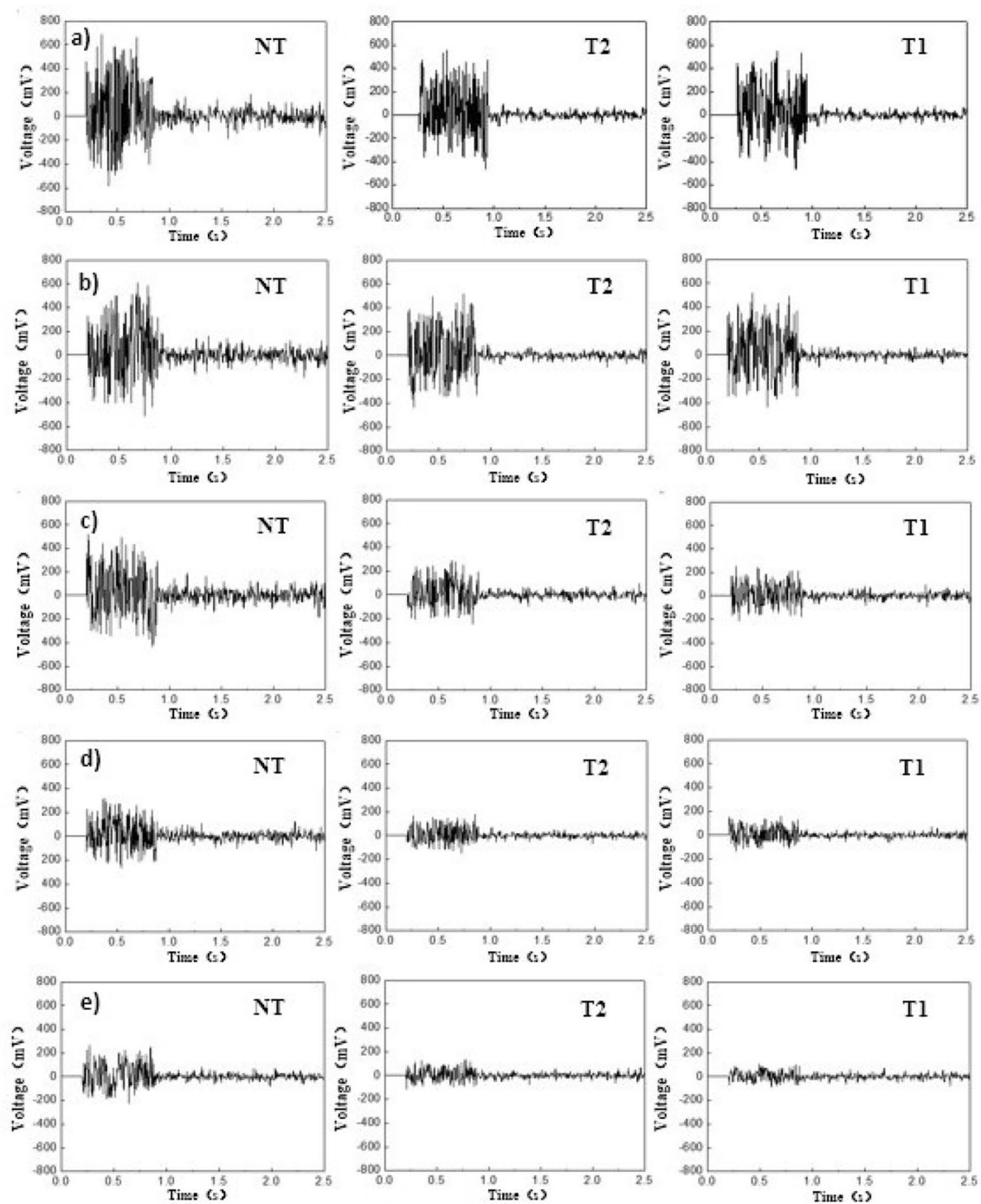
Figure 17 Acoustic emission energy output waveforms of three drill bits at different cutting speeds (v_c = 20, 30, 40, 50, and 60 m/min from top to bottom)

role of the pit micro-texture in the drilling process will decrease. Because the depth of T2 is greater than that of T1, it is less affected by bone chips than T1, resulting in gradually better performance after stable drilling than T1.

4.5 Discussion of Mechanisms
4.5.1 Anti-Friction Mechanism
The shear stress distribution x of the cutter-chip contact part on the cutter face can be expressed as Eq. (1):
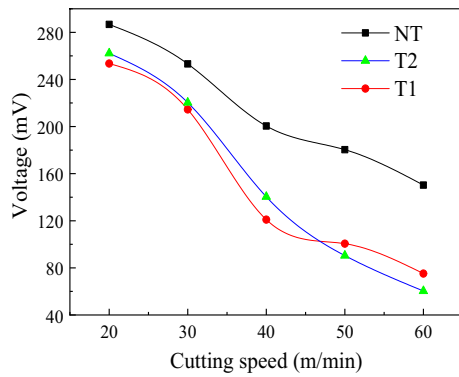
Figure 18 Mean voltage of three drill bits at different cutting speeds in front signal

$$\tau(x) = \begin{cases} \tau_s & 0 \le x \le l_{f1}, \\ \mu_2\sigma(x) & l_{f1} \le x \le l_{f2}, \end{cases} \tag{1}$$

where, τ_s is the shear yield strength of bone material, μ is the friction coefficient of sliding zone, x is the distance between workpiece and tool tip.

According to the theoretical basis of cutting, the normal stress distribution x function of the contact part between cutter and chip can be expressed as:

$$\sigma(x) = q(l_f - x)^\xi, \tag{2}$$

where, q is the stress equation coefficient, also is a constant, ξ is the stress distribution exponential coefficient, which is generally taken as 3 in drilling.

The positive pressure F_n acting on the front knife surface is:

$$F_n = \int_0^{l_f} \alpha_\omega\sigma(x)dx = \int_0^{l_f} \alpha_\omega\sigma_0\left(1 - \frac{x}{l_f}\right)^3 dx = \alpha_\omega\sigma_0\frac{l_f}{4}. \tag{3}$$

The shear force F_f in the knife-chip contact area is:

$$\begin{aligned} F_f &= \int_0^{l_f} \alpha_\omega\tau_s dx = \int_0^{l_f} \alpha_\omega\tau_s\left(1 - \frac{x - l_{f1}}{l_{f2}}\right)^3 dx \\ &= \alpha_\omega\tau_s l_{f1} + \alpha_\omega\tau_s\frac{l_{f2}}{4} = \alpha_\omega\tau_s\left(l_{f1} + \frac{l_{f2}}{4}\right). \end{aligned} \tag{4}$$

It can be understood from Eq. (4) that the positive pressure and shear force are directly proportional to the contact length and shear strength between knife and chip. Pits and convex hull reduce the contact length, thereby reducing the positive pressure and shear force, which in turn leads to a reduction in friction coefficient, achieving good friction reduction effect.
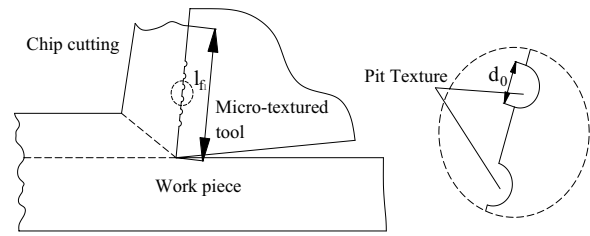
Figure 19 Simplified model of pit microtextured drill bits

4.5.2 Cooling Mechanism

The drilling temperature was primarily contributed by the heat generated and dissipated based on two aspects: the heat generated from drilling and the heat transfer mode analysis. During cortical bone drilling, the heat was primarily generated by the elastic-plastic deformation of the cortical bone material under the action of the drill bit, as well as by the friction among the cutting edge and front cutter surface, machined surface, and tool surface. The heat was primarily distributed on the cutting tool, cortical bone material, and chip [22]. Therefore, drilling heat can be reduced using one of two methods: (1) Reduce the heat generated or (2) accelerate cooling.

(1) Reducing Heat

As shown in Figure 19, once friction occurred between the bone chips and rake face, cutting heat was generated; subsequently, it was transferred to the bone chips and workpiece, as well as between the bone chips and drill bits in the form of heat flow [23, 24].
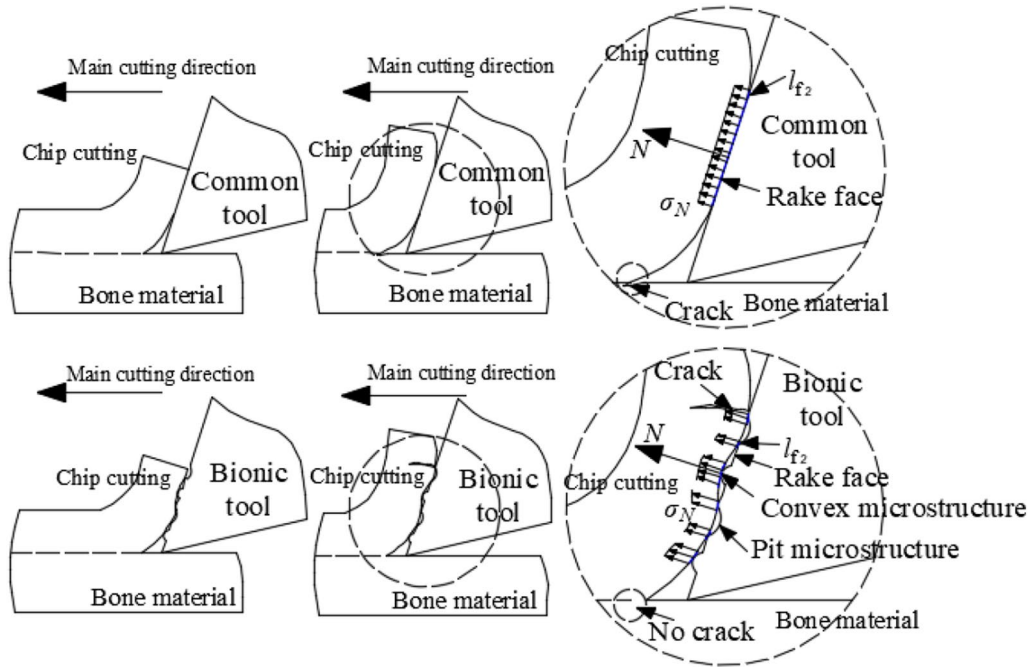
The cutting heat generated during the cutting of the bone material can be represented by the average temperature of the contact part between the drill bits and bone chip, which is generally calculated as follows:

$$\theta_t = \theta_s + \theta_f, \tag{5}$$

where θ_t is the average temperature of the cutter front surface, θ_s is the average temperature of the shear surface, and θ_f is the friction temperature of the cutter chip contact surface.

The average temperature of the contact area between the bone chips and microstructure drill bits is expressed as:

$$\begin{aligned} \theta_t' &= \frac{R_1 v_s \tau_s}{c_1 \rho_1 v \sin\phi} + \theta_0 + 0.754 R_2\overline{\tau}_c\sqrt{\frac{v l_f'}{\xi c_2 \rho_2 k_2}} \\ &= \frac{R_1 v_s \tau_s}{c_1 \rho_1 v \sin\phi} + \theta_0 + 0.754 R_2\overline{\tau}_c\sqrt{\frac{v(l_f - nd_0)}{\xi c_2 \rho_2 k_2}}, \end{aligned} \tag{6}$$

Lian *et al. Chinese Journal of Mechanical Engineering* (2023) 36:37

Page 11 of 13

Figure 20 Principle diagram of cutting bone material using typical drill bits and convex microstructure drill bits (top: typical drill bits; bottom: convex microstructure drill bits)

where τ_c is the average shear stress on the cutter, l_{f1} is the theoretical knife-chip contact length of the pit, ξ is the bone chip deformation coefficient, c_2 is the specific heat capacity of bone chip when the temperature is $(\theta_s+\theta_f)$, ρ_2 is the bone chip density when the temperature is $(\theta_s+\theta_f)$, k_2 is the bone chip thermal conductivity coefficient when the temperature is $(\theta_s+\theta_f)$, v_s is the shear speed, τ_s is the shear strength of the bone material, c_1 is the specific heat capacity of the average temperature of the bone materials, ρ_1 is the density of the bone material, v is the cutting speed, and θ_0 is the ambient temperature.

Because of the pits, the contact length between the bit and chip reduced, thereby reducing the heat generated during drilling.

(2) Increase in Heat Dissipation

The heat flux on the cutting surface of the tool is expressed as:

$$q_1 = (F_s + F_m)v_s/a_c a_w \cos \varphi. \tag{7}$$

The heat flux on the front cutter surface is expressed as:

$$q_2 = F_0 V_C/l_{f1} a_w. \tag{8}$$

The heat flow density on the rear cutter surface is expressed as:

$$q_3 = F_f v/l_{f1} a_w. \tag{9}$$

The total heat loss is expressed as:

$$Q_m = q_1 A_1 + q_2 A_2 + q_3 A_3 + Q_0, \tag{10}$$

where a_w is the bone chip width, also is the drilling thickness, φ is the shearing angle, F_0 is the friction between the front cutter surface and chip, F_s is the shear stress, F_m is the force required to change the chip momentum, and F_f is the frictional force on the rear cutter surface.

Owing to the pits, the heat dissipation area between the drill bit and cutting increased, and heat dissipation increased during drilling.

4.5.3 Crack Suppression Mechanism

The principle diagram of cutting bone materials using typical drill bits and convex-hull microstructured drill bits is shown in Figure 20.

Assuming that cracks occur during drilling and the half-length of microscopic cracks in bone material is a, the critical stress value generated by bone cracks is expressed as:

$$\sigma_c = \sqrt{\frac{2E\gamma}{\pi(1 - v^2)a}}. \tag{11}$$

The mean value of the positive stress at the knife–chip contact surface is expressed as:

$$\sigma_{\text{N}} = \frac{N}{a_{\text{w}} l_{\text{f}_2}}, \qquad (12)$$

where l_{f_2} is the theoretical knife-chip contact length of the convex hull, and N is the normal component of the cutting force on the contact surface.

When the microstructure of the convex hull is in contact with bone chips of higher flow properties, "derivative cutting" is likely to occur, which is conducive to the fracture of the chips on the bottom surface [25]. In addition, the convex hull microstructure shortens the actual contact length of the tool chips and increases the stress of the chips on the tool-chip contact surface [26, 27]. When the stress reaches the critical stress value σ_c, the chip breaks, which effectively inhibits the fracture of the bone material from generating fractured chips in the chip separation area that may expand along the bonding line [28]. The cracks were primarily affected by the external load, as well as temperature via the elastic strain energy. During drilling, the axial force is large, and the energy released through the formation and further expansion of cracks is also large.

Based on fracture mechanics, the energy release rate of the crack is expressed as:

$$G = \frac{1}{2} \frac{\partial}{\partial a} (W - U), \qquad (13)$$

where W and U are the change values of the external force and strain energy, respectively.

The pit microstructure reduced the contact area between the spiral cutting surface and workpiece; additionally, it reduced the contact length and hence the positive pressure and shear force on the contact surface, thereby reducing the coefficient of friction [29]. Therefore, the pit microstructure can effectively reduce friction, thereby reducing the occurrence of cracks.

Combined with the explanation in Section 4.2, it was clear that owing to the pits and convex hull, the triaxial force during drilling decreased significantly. Additionally, the contact length reduced during drilling, which decreased the positive pressure and shear force on the contact surface, thereby effectively reducing the external work. Meanwhile, the energy release of the crack was reduced, which reduced the generation of cracks.

5 Conclusions

In this study, the cooling and crack suppression performance of a bionic microtextured drill bit during the drilling of bone materials was evaluated. The following conclusions were obtained:

(1) A bionic microtextured bit can significantly improve drilling performance, effectively reduce the drilling force during drilling, and reduce the drilling heat as well as crack formation and diffusion.

(2) The pits in T1 and T2 shortened the tool-chip contact length and reduced the friction heat generated by drilling from the root. In addition, because of the pits, chips were easier to discharge and heat transfer occurred in a timelier manner, which effectively suppressed temperature increase during drilling and avoided thermal stress cracks. The cooling effect of T1 was better than that of T2.

(3) The convex hulls of T1 and T2 demonstrated good chip breaking ability, and the concave pit can store chips, which reduced the extrusion impact during drilling and inhibited the formation and propagation of cracks. The crack suppression effect of T2 was better than that of T1.

Author contributions
YSL was in charge of the whole trial; XDC performed the data analyses and wrote the manuscript; CX performed the experiment and data analyses; YYL and FL helped perform the analysis with constructive discussions; WZ and XYC guided the experiments. All authors read and approved the final manuscript.

Authors' Information
Yunsong Lian, born in 1986, is currently an associate professor and a master candidate supervisor at *Department of Mechanical and Electrical Engineering, Xiamen University, China*. His main research interests include energy saving cutting tool technology, bionic functional structure surface design, manufacturing and application, machining of refractory materials, and cutting tribology.
Xiande Chen, born in 1998, is currently a master candidate at *Department of Mechanical and Electrical Engineering, Xiamen University, China*.
Chaoping Xie, born in 1995, is currently a master candidate at *Department of Mechanical and Electrical Engineering, Xiamen University, China.*.
Yangyang Long, born in 1988, is currently a research assistant at *Institute of Dynamics and Vibration Research, Leibniz Universität Hannover, Germany*. His research interests include acoustics, radiology, nuclear medicine and medical imaging.
Fengtian Lin, born in 1987, is currently a project manager at *Xiamen Golden Egret Special Alloy Co., Ltd, China*.
Wei Zhou, born in 1982, is currently a professor and a PhD candidate supervisor at *Department of Mechanical and Electrical Engineering, Xiamen University, China*. His research interests include precision manufacturing technology, functional micro—structure manufacturing, new energy and energy saving technology, and MEMS.
Xuyang Chu, born in 1981, is currently an associate professor and a master candidate supervisor at *Department of Mechanical and Electrical Engineering, Xiamen University, China*. His main research interests include microfabrication technique, robotics and control.

References

[1] J B Sui, N Sugita, K Ishii, et al. Mechanistic modeling of bone-drilling process with experimental validation. *Journal of Materials Processing Technology*, 2014, 214: 1018−1026.

[2] Z R Liao, D Axinte, D Gao. On modelling of cutting force and temperature in bone milling. *Journal of Materials Processing Technology*, 2019, 266: 627−638.

[3] A Feldmanna, P Ganserb, L Noltea, et al. Orthogonal cutting of cortical bone: temperature elevation and fracture toughness. *International Journal of Machine Tools & Manufacture*, 2017, 118−119: 1−11.

[4] H Y He, C Y Wang, Y Zhang, et al. Investigating bone chip formation in craniotomy. *Proceedings of the Institution of Mechanical Engineers, Part H: Journal of Engineering Medicine*, 2017, 231: 959−974.

[5] J Lee, C L Chavez, J Prk. Parameters affecting mechanical and thermal responses in bone drilling: A review. *Journal of Biomechanics*, 2018, 71: 4−21.

[6] N Bertollo, H R M Milne, L P Ellis, et al. A comparison of the thermal properties of 2− and 3− fluted rills and the effects on bone cell viability and screw pull out strength in an ovine model. *Clinical Biomechanics*, 2010, 25(6): 613−617.

[7] H Heydari, N C Kazerooni, M Zolfaghari, et al. Analytical and experimental study of effective parameters on process temperature during cortical bone drilling. *Proceedings of the Institution of Mechanical Engineers, Part H: Journal of Engineering Medicine, Part H: Journal of Engineering in Medicine*, 2018, 232(9): 871−883.

[8] X S Li, W Zhu, J Q Wang, et al. Optimization of bone drilling process based on finite element analysis. *Applied Thermal Engineering*, 2016, 108: 211−220.

[9] N Sugita, L M Shu, T Shimada, et al. Novel surgical machining via an impact cutting method based on fracture analysis with a discontinuum bone model. *CIRP Annal-Manufacturing Technology*, 2017, 66(1): 65−68.

[10] L M Shu, S H Li, M Terashima, et al. A novel self-centring drill bit design for low-trauma bone drilling. *International Journal of Machine Tools & Manufacture*, 2020, 154: 103568.

[11] M F A Akhbar, A R Yusoff. Fast & injurious: Reducing thermal osteonecrosis regions in the drilling of human bone with multi-objective optimization. *Measurement*, 2020, 152: 107385.

[12] L F Wei. Study on friction properties and geometric parameters optimization of micro-textured tools for drilling cortical bone. *Tianjin University of Technology*, 2019. (in Chinese)

[13] G L Liu, C Z Huang, B Zhao, et al. Effect of machined surface integrity on fatigue performance of metal workpiece: A review. *Chinese Journal of Mechanical Engineering*, 2021, 34: 118.

[14] J A Robles-Linares, D Axinte, Z R Liao, et al. Machining-induced thermal damage in cortical bone: Necrosis and micro−mechanical integrity. *Materials & Design*, 2021, 197: 109215.

[15] Y Liu, Y Quan, C J Wu, et al. Single diamond scribing of SiCf/SiC composite: Force and material removal mechanism study. *Ceramics International*, 2021, 47: 0272−8842.

[16] R Fu, Z Y Jia, F J Wang, et al. Drill-exit temperature characteristics in drilling of UD and MD CFRP composites based on infrared thermography. *International Journal of Machine Tools & Manufacture*, 2018, 135: 24−37.

[17] G J Liu, Z C Zhou, X Qian, et al. Wear mechanism of cemented carbide tool in high speed milling of stainless steel. *Chinese Journal of Mechanical Engineering*, 2018, 31: 98.

[18] X Kong, Y M Wang, Q Yang, et al. Damage identification in fiber reinforced titanium matrix composites using acoustic emission. *Journal of Alloys and Compounds*. 2020, 826: 153928.

[19] Z Y Gao, J Lin, X F Wang, et al. Grinding burn detection based on cross wavelet and wavelet coherence analysis by acoustic emission signal. *Chinese Journal of Mechanical Engineering*, 2019, 32: 68.

[20] Z R Liao, D A Axinte. On monitoring chip formation, penetration depth and cutting malfunctions in bone micro-drilling via acoustic emission. *Journal of Materials Processing Technology*, 2016, 229: 82−93.

[21] Y Zhang, J F Shi, J Y Zheng. A method of fracture toughness JIC measurement based on digital image correlation and acoustic emission technique. *Materials & Design*, 2021, 197: 109258.

[22] Y Turki, M Habak, R Velasco, et al. Experimental investigation of drilling damage and stitching effects on the mechanical behavior of carbon/epoxy composites. *International Journal of Machine Tools & Manufacture*, 2014, 87: 61−72.

[23] J Kummel, D Braun, J Gibmeier. Study on micro texturing of uncoated cemented carbide cutting tools for wear improvement and built−up edge stabilisation. *Journal of Materials Processing Technology*, 2015, 215: 62−70.

[24] R D Han, J J Xi, H Wang. Fundamentals of metal cutting and cutting tools. Harbin:*Harbin Institute of Technology Press*, 2013. (in Chinese)

[25] Y J Lee, H Wang. Characterizing crack morphology toward improving ductile mode cutting of calcium fluoride. *Ceramics International*, 2021, 47: 28543−28556.

[26] Q Liu, Z R Liao, J Cheng, et al. Mechanism of chip formation and surface-defects in orthogonal cutting of soft-brittle potassium dihydrogen phosphate crystals. *Materials & Design*, 2021, 198: 109327.

[27] Z Yu, C P Li, X Y Qiu, et al. Study on damage in carbon fiber reinforced plastic drilling using step cutting mechanism drill. *Journal of Alloys and Compounds*, 2020, 826: 154058.

[28] Y J Zhen, Z Chong, F J Wang, et al. An investigation of the effects of step drill geometry on drilling induced delamination and burr of Ti/CFRP stacks. *Composite Structures*, 2020, 235: 111786.

[29] K Zeng, X Wu, F Jiang, et al. Experimental research on micro hole drilling of polycrystalline Nd: YAG. *Ceramics International*, 2021, 48(7): 9658−9666.